

**A FACILITY TO PRODUCE AN ENERGETIC, GROUND STATE ATOMIC OXYGEN BEAM
FOR THE SIMULATION OF THE LOW-EARTH ORBIT ENVIRONMENT**

Andrew D. Ketsdever, David P. Weaver and E.P. Muntz
Collaboration for Nonequilibrium Technologies
United States Air Force Phillips Laboratory and University of Southern California

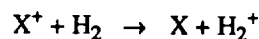
ABSTRACT

Because of the continuing commitment to activity in low-Earth orbit (LEO), a facility is under development to produce energetic atmospheric species, particularly atomic oxygen, with energies ranging from 5 to 80 eV. This relatively high flux facility incorporates an ion engine to produce the corresponding specie ion which is charge exchanged to produce a neutral atomic beam. Ion fluxes of around 10^{15} sec^{-1} with energies of 20-70 eV have been achieved. A geometrically augmented inertially tethered charge exchanger (GAITCE) was designed to provide a large column depth of charge exchange gas while reducing the gas load to the low pressure portion of the atomic beam facility. This is accomplished using opposed containment jets which act as collisional barriers to the escape of the dense gas region formed between the jets. Leak rate gains to the pumping system on the order of 10 were achieved for moderate jet mass flows. This system provides an attractive means for the charge exchange of atomic ions with a variety of gases to produce energetic atomic beams.

INTRODUCTION

Atomic oxygen is the predominant species in the low-Earth orbit (LEO) environment between 180 and 650 kilometers. Oxygen atoms, primarily in the ground (3P) state, results from the photodissociation of molecular oxygen by solar ultraviolet radiation. In the thermosphere ($> 80\text{km}$), it is present at nearly thermal energies ($\sim 0.01\text{eV}$); however, the relative kinetic energies encountered during collisions with spacecraft in LEO is about 5 eV with fluxes in the range of 4×10^{14} to $2 \times 10^{15} \text{ cm}^{-2} \text{ sec}^{-1}$ normal to the ram direction. Atomic oxygen is observed to be the major source of spacecraft material degradation and glow. Spacecraft which operate in LEO must be designed to withstand the adverse effect of atomic oxygen on sensitive optical instruments, solar arrays, and even structural components. Because of the observations of many satellite and Shuttle missions, several ground based facilities capable of reproducing the LEO environment were developed (ref. 1,2,3). Ground based systems are more adaptable, cost efficient, and practical than dedicated satellite missions.

With this in mind, the Department of Aerospace Engineering at the University of Southern California in conjunction with the United States Air Force's Phillips Laboratory has been developing a facility capable of producing a ground state, energetic O atom beam with energies and fluxes similar to those encountered in LEO (ref. 4,5). Figure 1 shows the general schematic of the energetic atomic beam facility at USC. Ion engine technology has been incorporated to produce a beam of energetic ions. Because the engine can be run on several gases, simulation of any atmospheric specie can be achieved; however, atomic oxygen is the specie of interest in this paper. The ions are accelerated to the desired energy range using electrostatic grids producing a well-collimated beam which is energy selected using a Wien filter (ref. 6). The remaining atomic ions undergo a charge exchange process in molecular hydrogen (large charge exchange cross section, small scattering angle per collision) in the reaction



to produce energetic atoms. In the USC facility, energies upwards of 80 eV with continuous fluxes estimated around 10^{15} sec^{-1} should be achievable. This places this facility in an operational energy region which is much higher than other facilities, using microwave discharges or laser discharges expanding through nozzles, whose energies may just reach 5 eV. Descriptions and results of the major system components are the main focus of this paper.

This work is supported by the Air Force Phillips Laboratory (A. Ketsdever-Palace Knight Program) and the University of Southern California.

BACKGROUND

The USC atomic beam facility consists of three major components. The first is the ion engine which consists of the hollow anode ring jet (HARJ) plasma source and a secondary discharge chamber. The second is the Wien energy filter which consists of an electromagnet and two electrostatic plates. The Wien filter is capable of rejecting ions produced in the ion engine which do not meet the experimental energy requirements. The Wien filter is described in detail in reference 6 and will not be discussed here. The final component is a geometrically augmented inertially tethered charge exchanger (GAITCE) which contains the dense charge exchange gas. The subsequent sections discuss the ion engine and GAITCE in detail.

Hollow Anode Ring Jet (HARJ) Plasma Source

In order to obtain an energetic beam of neutral atoms by the method outlined earlier, it is first necessary to produce the corresponding ion which can then be accelerated to the desired energy. Ions are formed using a hollow anode electrical discharge plasma source first investigated fifty years ago (ref. 7) for electron beam production in cathode ray tubes. Recently sources of this type have been used for electron beam welding and material processing. The hollow anode plasma source is contained inside a high vacuum facility with molecular oxygen fed into its discharge chamber. Neutrals, ions and electrons all emerge from the aperture in the anode with a relatively dense gas cloud formed in the vicinity of the anode aperture to accommodate a higher degree of ionization and dissociation. To accomplish this, the concept of an inertially tethered gas cloud formed by a ring jet (ref. 8) is used. A ring jet is a series of orifices or a continuous slot through which gas being supplied by a stagnation chamber flows. The orifices or slot are arranged so that their axes are at an angle ω to the normal of the plane defined by the ring. For the purposes of the hollow anode ring jet (HARJ) used here and shown on the left in Figure 2, the stagnation chamber is the hollow anode discharge chamber.

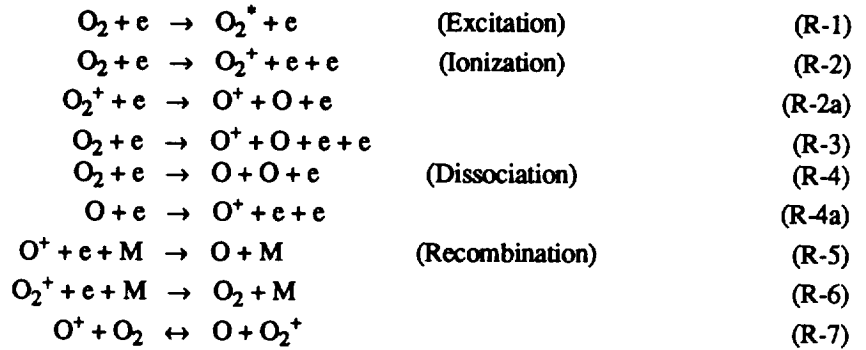
The HARJ exploits the low pressure, high voltage glow discharge, i.e. discharges operated on the left side of the Paschen curve. In a gas discharge of this nature when a potential is supplied to the cathode, electrons are emitted from the cathode material based on that material's work function. Each electron that leaves the cathode is accelerated toward the anode ionizing the gas in the discharge chamber on the way. Some of the positive ions produced drift towards the cathode and become sources of more electrons by secondary emission due to ion bombardment. The region of interest in this work is that of the abnormal glow with the Aston dark space, cathode glow, Crookes dark space, and the negative glow filling up parts of the discharge chamber. Electrons produced in the discharge have energies close to that corresponding to the cathode fall and are slowed both inside and outside of the anode. Maximum electron beam energy is obtained when the cathode fall occupies the entire discharge chamber; otherwise, the electrons are slowed in the negative glow region before exiting the chamber.

Typical pressures in the discharge chamber range from 1 to 150 $\mu\text{m Hg}$. At these pressures the discharge occurs for voltages from 1 kV to 5 kV with currents ranging from 10 - 200 mA. This range of discharge characteristics is consistent for a variety of gases such as O_2 , N_2 , Ar, CO_2 , Ne. The discharge voltage has an upper bound which is determined by the temperature the hardware can withstand and by the transition from a glow discharge to the undesired arc discharge. The input power, discharge chamber pressure, and chamber geometry all must be considered when attempting to determine the degree of ionization. In the schematic shown in Figure 2, the plasma is given a preferred direction by the ring jet angle $\omega = 45^\circ$. The source has a stainless steel cathode surrounded by ceramic insulators. The anode is made of aluminum and water cooled to reduce the HARJ operating temperature. The working gas is introduced into the discharge chamber through small radially positioned orifices in the anode cone.

The new generation HARJ has several interesting features. First, the source is omnivorous and can be operated with several different discharge gases. Only the discharge pressure and input power need to be modified for optimum operating conditions. Second, there appears to be no serious erosion of the cathode material due to high energy ion bombardment over several hours of operation. Third, there are no problems starting the discharge. The discharge initiates spontaneously at low currents ($\sim 10\text{mA}$), and the current increases in a controlled manner as the voltage to the discharge is increased. Transition from a glow discharge to an arc discharge is not observed for this source operating at up to 200 mA. Finally, the source is simple in design and easy to operate.

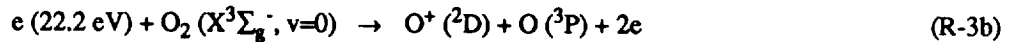
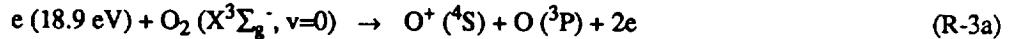
Reactions in an Oxygen Discharge

In a discharge of the type mentioned earlier, several chemical processes are available to electron-molecule or electron-atom collisions. Among these are



This set of reactions is by no means complete and is only meant to show some of the more important reactions taking place within the discharge. Of particular importance are the ionization processes of reactions (R-2), (R-2a), (R-3), and (R-4a) and the ion destruction processes of reactions (R-5) and (R-6). From the ionization cross sections given in reference 9, it is clear that the (R-2) \rightarrow (R-2a) branch for the creation of atomic ions is preferred over the direct dissociative ionization of reaction (R-3) for the range of electron energies from 50-300 eV. The ionization cross-section for reaction (R-4a) is approximately $1.5 \times 10^{-16} \text{ cm}^2$ for an incident electron energy of 100 eV (ref. 10). A consequence of the relatively high cross-sections for reactions (R-2) and (R-2a) is that the emerging beam will have a considerable part of its total current produced by molecular ions. The relative portion of the total beam current produced by O^+ ions can be reasonably approximated by the ratio of the cross-sections $q_i(\text{R-2}) / \{q_i(\text{R-2}) + q_i(\text{R-3})\}$ yielding about 35%.

Figure 3 shows the fraction of oxygen ions in an excited state (ref. 11) being produced by a gas discharge source similar to the one used for this study. The vast majority of the ions produced in both cases are in the ground states for incident electron energies less than 20 eV. However, this fraction of ions in an excited electronic state rises to about 30% for electron energies greater than 50 eV. The ionization reactions (R-3) can be further broken down by (ref. 12)



Reaction (R-3a) results in the formation of ground state ions by electrons which are 6.84 eV above the 12.06 eV ionization potential. The energy difference between ground $\text{O}^+(^4\text{S})$ and the first excited state $\text{O}^+(^2\text{D})$ is 3.32 eV. Thus, the minimum electron energy required to produce excited $\text{O}^+(^2\text{D})$ ions in reaction (R-3b) is 22.2 eV. As can be seen in Figure 4, the jump in relative concentration of electronically excited ions produced in a gas discharge source occurs near 20 eV.

Lindholm and Gustafsson (ref. 13) have also found that O^+ ions produced in discharge sources from CO , N_2O , and CO_2 have different properties. In beams from CO_2 the ground state ions seem to be more prevalent than the metastable $\text{O}^+(^2\text{D}, ^2\text{P})$ states. Beams from CO and N_2O as well as O_2 appear to maintain the metastable ($^2\text{D}, ^2\text{P}$) states as equally important. The importance of the electronic states of the ions becomes evident when cross sections for the ions neutralization to form O atoms is investigated.

Incorporation of the HARJ into an Ion Engine

Although the HARJ produces a relatively large degree of ionization by itself, nearly 60% of the oxygen molecules will escape the HARJ discharge chamber and ring jet flow field un-ionized. For this reason and to allow for acceleration of the ions produced, the HARJ has been incorporated into an ion engine assembly shown in Figure 2. Beyond the exit of the HARJ discharge chamber, the partially ionized plasma forms an inertially tethered gas cloud (due to the ring jet configuration) whose charged particles are partially contained in a secondary discharge volume. In this second discharge, an external electric and magnetic field increases the number of collisions creating a higher degree of ionization and a higher fraction of dissociated molecules.

The positive potential supplied to the secondary discharge volume's anode accelerates the electrons to energies capable of ionizing and dissociating the molecular oxygen. The magnetic field is set up by permanent magnets radially positioned around the anode. The magnetic field strength was designed such that the electrons emerging from the HARJ would acquire a radius of gyration

$$r_g = \frac{mv_{o\perp}}{qB} \quad (1)$$

(where m is the particle mass, v_{\perp} is the velocity perpendicular to B , and B is the magnitude of the magnetic field) on the order of the secondary discharge volume radius. This increases the electrons path length to a few mean free paths within the secondary volume allowing more time for collisions with gas particles. The ions produced in the ion engine are then extracted from the secondary discharge volume through the use of electrostatic grids forming an energetic ion beam. This beam must then be energy selected and neutralized to be of use for degradation studies.

Ion Charge Exchange Process

Because of the near resonant charge exchange situation (implying a large charge exchange cross section) and the beneficial 16:1 mass ratio, (implying a small scattering angle) atomic hydrogen is a very attractive charge exchange target gas. However, it is difficult to produce and maintain pure hydrogen atom gas clouds. Cross sections for oxygen ion charge exchange in molecular hydrogen have also been investigated. This process may indeed have two branches due to the added modes introduced by the hydrogen molecule. These branches are



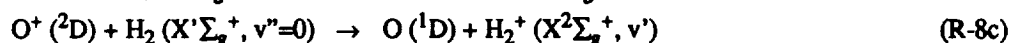
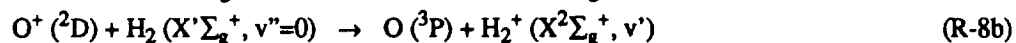
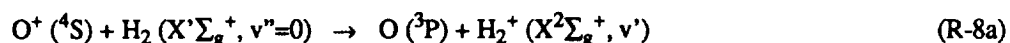
and



where the energy defect for (R-8) for ground state ions and molecules is $\Delta E = 1.81$ eV. Obviously if the process expressed by (R-9) dominates the flow field chemistry, molecular hydrogen must be excluded as a viable charge exchange gas.

Previous studies (ref. 14,15) have concluded that (R-9) is the major branch for oxygen ions with incident energy near thermal energies (~ 0.01 eV). The rate constant found in reference 9 for reaction (R-9) obtained from a gas discharge on CO_2 (i.e. mostly ground state O^+ ions produced) was 1.58×10^{-9} cm^3/sec which is in reasonable agreement with the other studies at thermal energies. *Kim, et al.* (ref. 15) found evidence that the rate constant for reaction (R-9) is decidedly less for gas discharges on O_2 than it is for CO_2 discharge. This was found to be caused by the relatively high percentage of metastable ions (^2D , ^2P) produced by gas discharge sources operating on pure molecular oxygen (ref. 11). Therefore, the electronically excited O^+ (^2D , ^2P) ions have a significantly smaller reaction rate constant than ground state (^4S) ions at thermal energies. As mentioned earlier, the HARJ is expected to produce anywhere from 20 - 40% of metastable oxygen ions. This fact coupled with incident ion energies, which are an order of magnitude or two larger than thermal energies (and enough to overcome the energy defect of 1.81 eV), indicates that the reaction branch (R-9) will probably be negligible.

The charge exchange reaction (R-8) can be further described by



The energy defect for reaction (R-8a) is 1.81 eV which is sufficiently large that the probability of charge transfer is small. Reaction (R-8b) only has an energy defect of about 0.1 eV when the product ion vibrational level v' is 6 or 7. For $v'=0$ in reaction (R-8c), the energy defect is 0.46 eV. Due to the low ΔE for (R-8b) and (R-8c), the cross sections for these reactions are expected to be large. The charge exchange cross-sections for reaction (R-8a) have been experimentally determined by a variety of sources. Figure 4 (ref. 12,13) shows the relative cross sections for the reactions (R-8b,c) as a function of the incident ion kinetic energy for metastable ions formed in the discharge. As Figure 3 shows, the amount of metastables produced is dependent on the electron energy. Above about 25 - 30 eV, the relative concentration of metastable ions is around 30%. Figure 4 shows that the cross section for charge exchange is larger for the metastable ion reactions than that of the ground state. This is consistent with the statements made earlier in the section. The ratio of the charge exchange cross sections for atomic and molecular hydrogen, up to large ion energies, ranges from about 1 to 2 indicating that not much is lost using molecular hydrogen as the charge exchange gas. Cross sections for various ion/molecule charge exchange and scattering collisions are shown in Table 1.

The creation of fast neutral species, for the case of fast ions impinging on a cloud of charge exchange gas is given by (ref. 4)

$$d(n_{\text{of}}) = (n_{\text{if}} Q_{\text{ce}} - n_{\text{of}} Q_{\text{ion}} - n_{\text{of}} Q_{\text{sc}}) d(L_n) \quad (2)$$

where n_{of} is the number density of the fast neutrals produced, n_{if} is the number density of the fast incoming ions, L_n is the column depth of charge exchange gas, and Q_{ce} , Q_{ion} , and Q_{sc} are the charge exchange, ionization, and scattering cross sections.

It is assumed that $n_{or}=0$ when $I_n=0$, and that a near-resonant process is taking place, i.e. $Q_{ion} \ll Q_{ce}$. The solution to (2), using the results in Table 1 for O^+/H_2 charge exchange, gives the maximum degree of neutralization as nearly 45% which occurs for a column depth of charge exchange gas of $1.44 \times 10^{15} \text{ cm}^{-2}$. This assumes that two scattering collisions are allowed for the entire process. This column depth must be maintained within the central region of the GAITCE in order to produce a high neutral atom yield

Geometrically Augmented Inertially Tethered Charge Exchanger (GAITCE)

The ions which pass through the Wien filter undergo a charge exchange process via collisions with a charge exchange gas within the confines of the geometrically augmented inertially tethered charge exchanger (GAITCE) producing a neutral atomic beam. The GAITCE configuration is shown in Figure 5. In a typical experiment, reducing the mass flow of charge exchange gas into the vacuum system is always of interest. The charge exchange gas is introduced to the GAITCE geometry by opposed jets, with the jet flows acting as collisional barriers to the escape of relatively dense gas trapped in the central region. The GAITCE is differentially pumped to remove the gas which has passed through the perforated pumping screen and no longer available for charge exchange. Skimmers are added in the flow field to further aid in the containment process. This design allows for a column depth of charge exchange gas adequate for a high degree of neutralization while minimizing the mass flow to the high vacuum portion of the atomic beam pumping system.

The opposed containment jets of the GAITCE are basically free jets expanding into a relatively low-density (compared to the jet stagnation density) background gas. The density of the free jet flowfield decreases as the inverse square of the distance R from the source as measured along a streamline. The density varies from streamline to streamline by (ref. 16)

$$\frac{\rho(R, \theta)}{\rho(R, 0)} = \cos^2\left(\frac{\pi\theta}{2\phi}\right) \quad (3)$$

where R is the distance from the source measured along a streamline, θ is the angle of the streamline measured from the source center line, and ϕ is a constant based on the gas used ($\phi = 1.365$ for $\gamma = 1.67$ and 1.662 for $\gamma = 1.40$). A simple physical model for free jet penetration into a background gas has been developed by *Muntz, et al.* (ref. 17). The background gas density is reduced from its equilibrium value far from the containment jet by collisions with jet species.

An important dimension in this formulation is the distance from the jet at which the background density has been reduced by $1/e$ of its value far away from the jet. This distance is known as the radius of penetration, r_p . As a function of θ from the jet centerline, r_p is given by (ref. 17)

$$r_p(\theta) = \left(\frac{V_{rel}}{C_B}\right) \pi \sigma_{JB}^2 n_{Jo} c_J(\gamma) D_o^2 \cos^2\theta \quad (4)$$

where

$$V_{rel} = v_{J\infty} + C_B ; \quad v_{J\infty} = \sqrt{\frac{2\gamma kT_J}{\gamma - 1 m_J}} ; \quad C_B = \sqrt{\frac{8kT_B}{\pi m_B}} ; \quad \sigma_{JB} = \frac{\sigma_J + \sigma_B}{2}$$

Here, $v_{J\infty}$ is the jet limit velocity, C_B is the mean thermal speed of the background gas, σ_{JB} is the combined collision diameters, n_{Jo} is the jet stagnation number density, D_o is the jet orifice diameter, and $c_J(\gamma)$ is a constant ($c_J(\gamma) = 0.15$ for $\gamma = 1.67$ and 0.0863 for $\gamma = 1.40$), m_J and m_B are the mass of the jet and background gases, and T_J and T_B are their temperatures, respectively.

The radius of penetration can be nondimensionalized by D_o to give $R_p = r_p / D_o$. For conditions where $R_p < 1$, the background gas begins to penetrate the jet flowfield up to the jet itself. For the application of background gas containment by opposed jets, which is of interest here, it is important to keep $R_p \gg 1$ or $r_p \gg D_o$. As can be seen from equation (4), $r_p(\theta)$ goes to zero as θ approaches 90° . Thus, the background gas can penetrate and in fact escape the central region of the GAITCE through the skimmer openings of the charge exchanger at these large angles causing "leaks" to the high vacuum portion of the system. To counter this adverse effect, the containment jets were positioned on traverses so that the angle θ to the edge of the skimmer openings of the charge exchanger could be varied.

There are two competing factors which determine the most efficient jet placement along the GAITCE centerline (z -direction). The first is the amount of the jet mass flow, \dot{M}_{jet} , which is rejected by the skimmer, thus not entering the central region of the GAITCE. As z increases and thus θ ($\theta = \tan^{-1}(R_{opening}/z)$) decreases, the jet flow which does not enter the skimmer, \dot{M}_{ne} , increases as equation (3) suggests. \dot{M}_{ne} is lost to the chamber pumping system. This factor is counteracted by the

effect of the radius of penetration. As z increases, the effective radius of penetration in the direction of the edge of the skimmer opening, $r_{p,edge}$, increases as equation (4) shows. A larger $r_{p,edge}$ implies more containment of the background gas in the central region of the GAITCE is expected. Because the jet stagnation number density is a governing parameter of r_p , larger values of M_{jet} are also expected to contain more efficiently.

EXPERIMENTAL FACILITY

The atomic beam facility is cryogenically pumped using gaseous (24-26 K) helium and is capable of maintaining pressures of about 1×10^{-5} Torr when the mass flow from all sources is 20 mg/sec. This vacuum facility is backed by two large diffusion pumps (8500 l/sec) and a 1000 l/s turbopump to remove any incondensibles. The facility is fitted with a variety of instrumentation and diagnostic tools including a quadrupole mass spectrometer, an electron beam, a baratron with scanning valve capable of reading multiple pressure ports, and a traversing system capable of moving the entire length of the chamber.

The first step in acquiring experimental data was to investigate the discharge characteristics of the ion engine. An electrostatic energy analyzer (EEA) was used to obtain the ion energy distributions and fluxes as a function of the ion engine parameters (p_{dc} , I_{dc} , I_{sd} , and V_{acc}). The EEA probe is shown in Figure 6. It is similar in design to the one used by *Lipschultz, et al.* (ref. 18) in that it has a three grid assembly preceding the collection cup. The first grid, G1, is used to repel unwanted species, namely electrons. For this study it is kept at the same potential as the ion engine accelerating grid (V_{acc}) so that the incident ions are not accelerated in the probe. The bias V_2 to the second grid, G2, is varied to limit the collection of positive ions to those with a velocity greater than

$$v_c = -\sqrt{\frac{2q(V_2 - V_p)}{m_i}} \quad (5)$$

where q is the elemental charge, V_p is the local plasma potential, and m_i is the ion mass. The last grid, G3, is normally biased to suppress secondary electron emission from the collecting cup. However, previous work using the EEA have shown little evidence of a secondary emission. Therefore, the potential on grid 3 and the collecting cup are normally held at V_{acc} so that no ion acceleration takes place within the probe. The EEA ion current measurements are used to estimate the total ion flux from the engine.

Next, the GAITCE was investigated as a stand alone component. The general experimental set up for the charge exchanger is shown in Figure 5 with one exception. In the experimental configuration, the back opening of the GAITCE was blocked off (GAITCE length = 50.2 cm) with the reflection of molecules off the back wall modeling the presence of an opposing jet. The differential pumping of the central region is done through a perforated cylinder to evenly distribute the pumping throughout. Two pumping ports on the side of the GAITCE are open to the chamber in this experiment because of the availability of a large cryopump. However as a component in an atomic beam system, the charge exchanger will be differentially pumped by a high throughput turbopump. Typically the open area of the perforated cylinder is half of the combined pumping port area. Although charge exchange with molecular hydrogen is desired, molecular nitrogen is used as a model gas in this experiment due to cryopumping restrictions

The containment jet is mounted on a traverse which allows movement in the z -direction on the GAITCE centerline. A skimmer of half-angle 30° is attached to the front of the GAITCE to aid in containing the background gas. The skimmer was made from available materials; thus, the half-angle was not considered in the initial design. For future work, there may be an advantage to matching the skimmer angle to the angle from the jet (at some position, z) to the edge of the front opening. The containment jet diameter, D_o , is 0.246 cm, and the diameter of the front opening of the GAITCE is nearly 7.0 cm. Note that the jet diameter is only a few percent of the skimmer opening diameter; thus, the blockage of ions, caused by the presence of the jet, into the GAITCE is negligible. Pressure inside the central region and outside the pumping cylinder are recorded using an MKS baratron with a scanning valve. An impact pressure probe provided pressure readings outside the skimmer opening of the GAITCE. Generally, the probe was one skimmer opening radius downstream (+ z -direction) of the opening from the charge exchanger and able to traverse in the + x -direction, giving pressure profiles across the skimmer opening.

RESULTS

Ion Engine

Figure 7 shows the HARJ discharge chamber voltage versus current characteristic curve (no secondary discharge). As the voltage is increased, the current across the discharge chamber increases steadily and in a well-behaved manner. The locus of

points of the characteristic curve shift to the right as the HARJ discharge chamber pressure increases. The transition from a high voltage, low current glow discharge to the low voltage, high current arc discharge was not seen in the pressure and voltage ranges used in this experiment. After an initial warm up period of a few minutes, the HARJ discharge current remained relatively constant over a period of several hours. The source has run consistently for over 100 hours without any servicing.

Figure 8 shows a typical EEA current (I_{probe}) versus the potential on the second grid, V_2 , for $p_{dc}=100 \mu\text{m Hg}$, $I_{dc}=50 \text{ mA}$, $I_{sd}=100 \text{ mA}$, and $V_{acc}=0 \text{ V}$. The EEA was positioned one secondary discharge radius downstream of the accelerating grid. Normalized energy distributions also shown in Figure 12 are derived from

$$E(V_2) = \left[\frac{d(I_{probe})}{dV_2} \right] / E_{max}. \quad (6)$$

The energy distribution has a defined peak at 20 eV with a full-width half maximum of about 8 eV. By increasing I_{sd} by a factor of two, the total ion current from the ion engine increases by a factor of 2.25 and increases by more than a factor of 4 by tripling I_{sd} . The ion flux of positive ions per unit area per second is then easily calculated by dividing the probe current by the factor ($e A_p$) where e is the elemental charge and A_p is the area of the probe collection cup (3.14 cm^2). Ion fluxes obtained at these experimental conditions range from 0.66 to $2.7 \times 10^{12} \text{ cm}^{-2} \text{ sec}^{-1}$. The total ion flux per second over the entire discharge volume ranges from 0.29 to $1.2 \times 10^{15} \text{ sec}^{-1}$.

The ion current measurements can be significantly modified by shielding the teflon exterior of the EEA to reduce repulsion due to space charging. Also the assumption made above was that the EEA was completely accessible to incident ions; however, each of the three grids is only about 50% transparent. Without careful alignment of the grid mesh, blockage of the cup may be on the order of 75-85%. This suggests that the flux estimates made earlier may be a factor of 2-4 too low.

Charge Exchanger

The GAITCE performance is measured by the observed gain in background gas containment using the containment jet configuration over a configuration with the same central region pressure where the gas is able to diffuse freely from the neutralizer's interface with the high vacuum. The gain is given by

$$Gain(\dot{M}_{jet}, z) = \frac{\dot{M}_{diff}}{\dot{M}_{esc} + \dot{M}_{ne}} ; \quad \dot{M}_{diff} = m_B \frac{n_{cr} C_B}{4} A_o \quad (7)$$

where \dot{M}_{diff} is the mass flow diffusing out the skimmer opening assuming no containment jet is used, \dot{M}_{esc} is the mass flow escaping out the skimmer opening with the jet operating, as interpolated from an impact pressure probe measurement, $\dot{M}_{esc} + \dot{M}_{ne}$ represents the load on the vacuum system, m_B is the background gas molecule mass, n_{cr} is the background gas number density in the GAITCE central region, and A_o is the skimmer opening area. \dot{M}_{diff} is essentially constant over a reasonable range of the jet's position.

Figure 9 shows the gain as a function of z and \dot{M}_{jet} for a nitrogen ($\gamma=1.40$) gas flow. As expected the gain increases for a given mass flow by increasing z a moderate amount ($\sim 0.6 \text{ cm}$). Also plotted is $r_{p,edge}$ nondimensionalized by the distance from the jet to the skimmer edge d_{edge} . At small values of z , the effect of increasing $r_{p,edge}$ dominates the gain equation. However as z increases, \dot{M}_{ne} takes over as the major loss to the chamber pumping system.

CONCLUSIONS

Figure 9 suggests that reductions of the leak rate from the GAITCE to the high vacuum portion of the beam system can approach a factor of 10 for moderate \dot{M}_{jet} . This is a tremendous benefit to systems which require low chamber background pressures to maintain beam collimation and physical properties such as internal states and neutral atomic species. As anticipated the gain increases as $r_{p,edge}$ and \dot{M}_{jet} increase. Increases in \dot{M}_{jet} act to increase r_p across the entire skimmer opening thus increasing the relative background gas containment. The GAITCE makes an attractive charge exchanger for atomic oxygen ions with molecular hydrogen.

Previous studies (ref. 19) have indicated that the ion beam produced by the ion engine under consideration here has nearly a 1:1 ratio of molecular ions to atomic ions. Therefore, if the molecular ions are removed from the beam, this implies that approximately half of the ion flux produced by the ion engine will be removed from the flow field. If the ion energy distribution of the O^+ ions is narrowed to $\pm 1 \text{ eV}$ in the Wien filter, the ion flux is expected to be reduced by about an order of magni-

tude. The maximum possible conversion of the remaining ions to fast neutrals using molecular hydrogen as a charge exchange gas is only about 45%, further reducing the atomic beam flux. In order to achieve a fast neutral flux on the order of 10^{15} sec^{-1} an initial flux of ions of $5 \times 10^{16} \text{ sec}^{-1}$ must be produced by the ion engine taking these reductions into consideration. This is about an order of magnitude higher than the ion flux measured for the ion engine currently in the atomic beam facility. Significant improvements in the flux (up to 10x) can be expected from the next generation of ion engines by designing a larger plasma source and by running the source at higher discharge currents.

REFERENCES

1. Cross, J. and Blais, N., "High Energy/Intensity CW Atomic Oxygen Beam Source," *Rarefied Gas Dynamics, Progress in Aeronautics and Astronautics*, Vol. 116, AIAA, Washington D.C., 1989, pp. 143-155.
2. Caledonia, G., Krech, R., Upschulte, B., Sonnenfroh, D., Oakes, D. and Holtzclaw, K., "Fast Oxygen Atom Facility for Studies Related to Low Earth Orbit Activities," AIAA Paper 92-3972, 1992.
3. Stidham, C., Stueber, T., Banks, B., Dever, J., Rutledge, S. and Bruckner, E., "Low Earth Orbital Atomic Oxygen Environmental Simulation Facility for Space Materials Evaluation," NASA Tech. Memorandum 106128, 1993.
4. Ketsdever, A., Weaver, D. and Muntz, E.P., "A Molecular Hydrogen Ring Jet Charge Exchanger for the Production of Energetic Oxygen Atoms," AIAA Paper 94-0371, 1994.
5. Muntz, E.P., Boyd, I. and Ketsdever, A., "Rarefied Flow Testing in the 1990's: Measuring Those Phenomena that are Difficult to Calculate," AIAA Paper 94-2631, 1994.
6. Teal-Quiros, E., and Prelas, M., "New Tilted-Poles Wien Filter with Enhanced Performance," *Review of Scientific Instruments*, 60(3), 1989, pp. 350-357.
7. Dugdale, R., Maskrey, J., Ford, S., Harmer, P. and Lee, R., "Glow Discharge Beam Techniques," *Journal of Material Science*, 4, 1969, pp. 323-335.
8. Muntz, E. P., Kingsbury, D., De Vries, C., Brook, J. and Calia, V., "Inertially Tethered Clouds of Gas in a Vacuum," *Rarefied gas Dynamics*, B. G. Teubner Stuttgart, Germany, 1986, pp. 474-485.
9. Farchi, A., Aubert, J., Wartski, L., Coste, P. and Mardirossian, C., "A Broad Beam Microwave O^+ Ion Source," *Journal of Physics D*, 25(7), 1992, pp. 1149-1151.
10. Heinrich, F., Stoll, H., Scheer, H. and Hoffmann, P., "Energy Analysis of Neutral Atoms in Broad Oxygen Ion Beams by Doppler-Shift Measurements," *Journal of Applied Physics*, 68(11), 1990, pp. 5428-5434.
11. Turner, B., Rutherford, J. and Compton, D., "Abundance of Excited Ions in O^+ and O_2^+ Ion Beams," *Journal of Chemical Physics*, 48(4), 1968, pp. 1602-1608.
12. Moran, T. and Wilcox, J., "Charge Transfer Reactions of Ground $O^+(^4S)$ and excited $O^+(^2D)$ State Ions with Neutral Molecules," *Journal of Chemical Physics*, 69(4), 1978, pp. 1397-1405.
13. Gustafsson, E. and Lindholm, E., "Ionization and Dissociation of H_2 , N_2 , and CO in Charge Exchange Collisions with Positive Ions," *Arkiv för Fysik*, 18(13), 1960, pp. 219-239.
14. Smith, D., Adams, N. and Miller, T., "A Laboratory Study of the Reactions of N^+ , N_2^+ , N_3^+ , N_4^+ , O^+ , O_2^+ , and NO^+ Ions with Several Molecules at 300 K," *Journal of Chemical Physics*, 69(1), 1978, pp. 308-318.
15. Kim, J., Theard, L. and Huntress, W., "ICR Studies of Some Hydrogen Atom Abstraction Reactions: $X^+ + H_2 \rightarrow XH^+ + H$," *Journal of Chemical Physics*, 62(1), 1975, pp. 45-52.
16. Ashkenas, H. and Sherman, F., "The Structure and Utilization of Supersonic Free Jets in Low Density Wind Tunnels," *Rarefied Gas Dynamics*, Academic Press, New York, 1966, pp. 84-105.
17. Deglow, T. and Muntz, E.P., "Isotope Separation by Jet-Background Interaction," *Journal of Applied Physics*, 50(2), 1970, pp. 589-594.
18. Lipschultz, B., Hutchinson, I., LaBombard, B. and Wan, A., "Electric Probes in Plasmas," *Journal of Vacuum Science Technology A*, 4(3), 1986, pp. 1810-1816.
19. Pham-Van-Diep, G., Muntz, E. P. and Weaver, D., "Ring-Jet Neutralization of Low Energy Oxygen Ion Beams," *Rarefied Gas Dynamics*, VCH, 1991, p. 1553.

Table 1. Charge Exchange and Scattering Cross Sections for Collisions Partners at 10 eV

Charge Exchange Partners	Q_{ce} ($\times 10^{-16} \text{ cm}^2$)	Q_{sc} ($\times 10^{-16} \text{ cm}^2$)	θ_{max} (degrees)
O^+ in O_2	5.0	8.0	> 90
O^+ in O	35	5.0	90
O^+ in H	16	3.0	3.5
O^+ in H_2	9.0	6.9	7.5
O_2^+ in O_2	30	10	90
N_2^+ in N_2	35	12	90

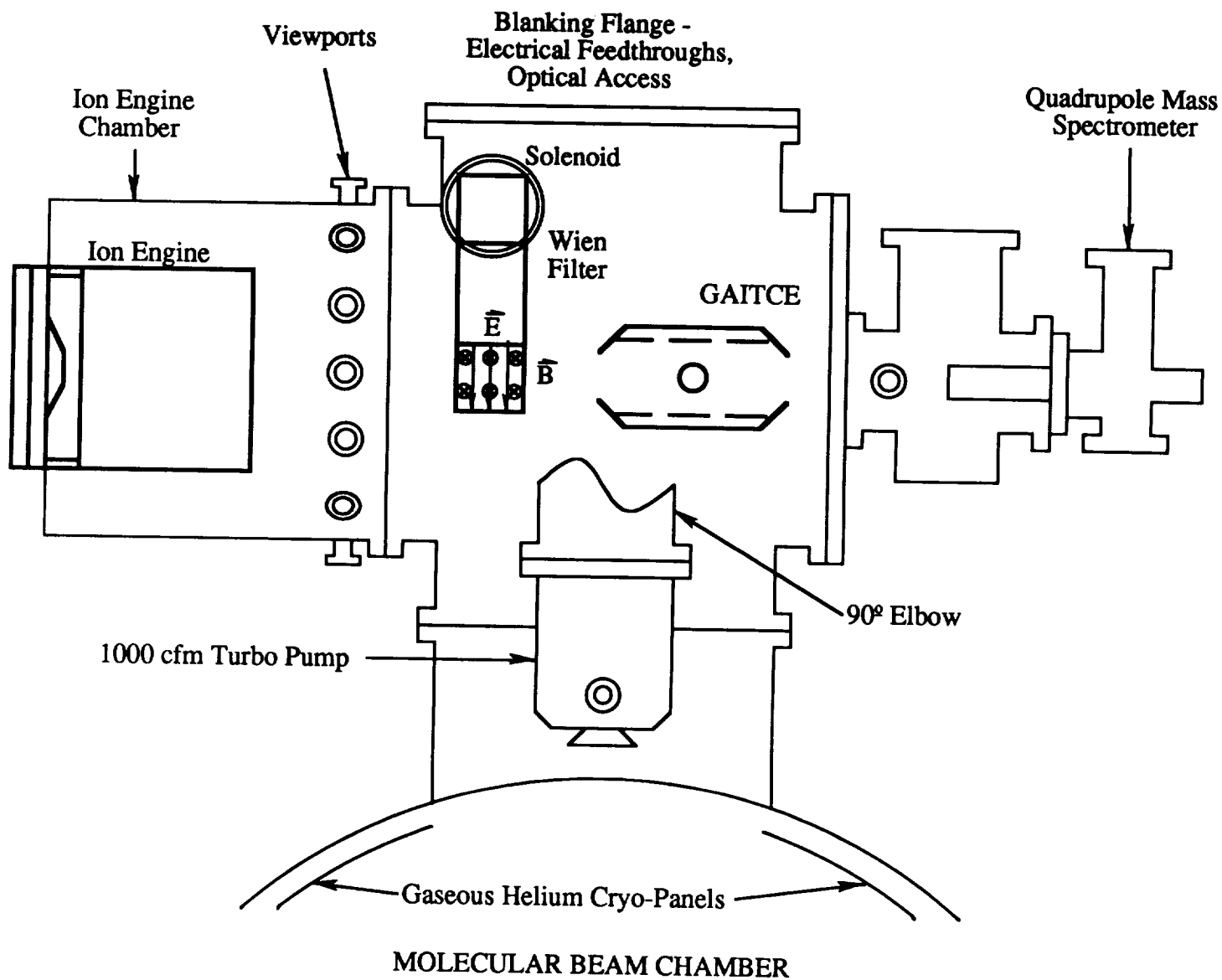


FIGURE 1

USC/Phillips Laboratory Atomic Beam Facility

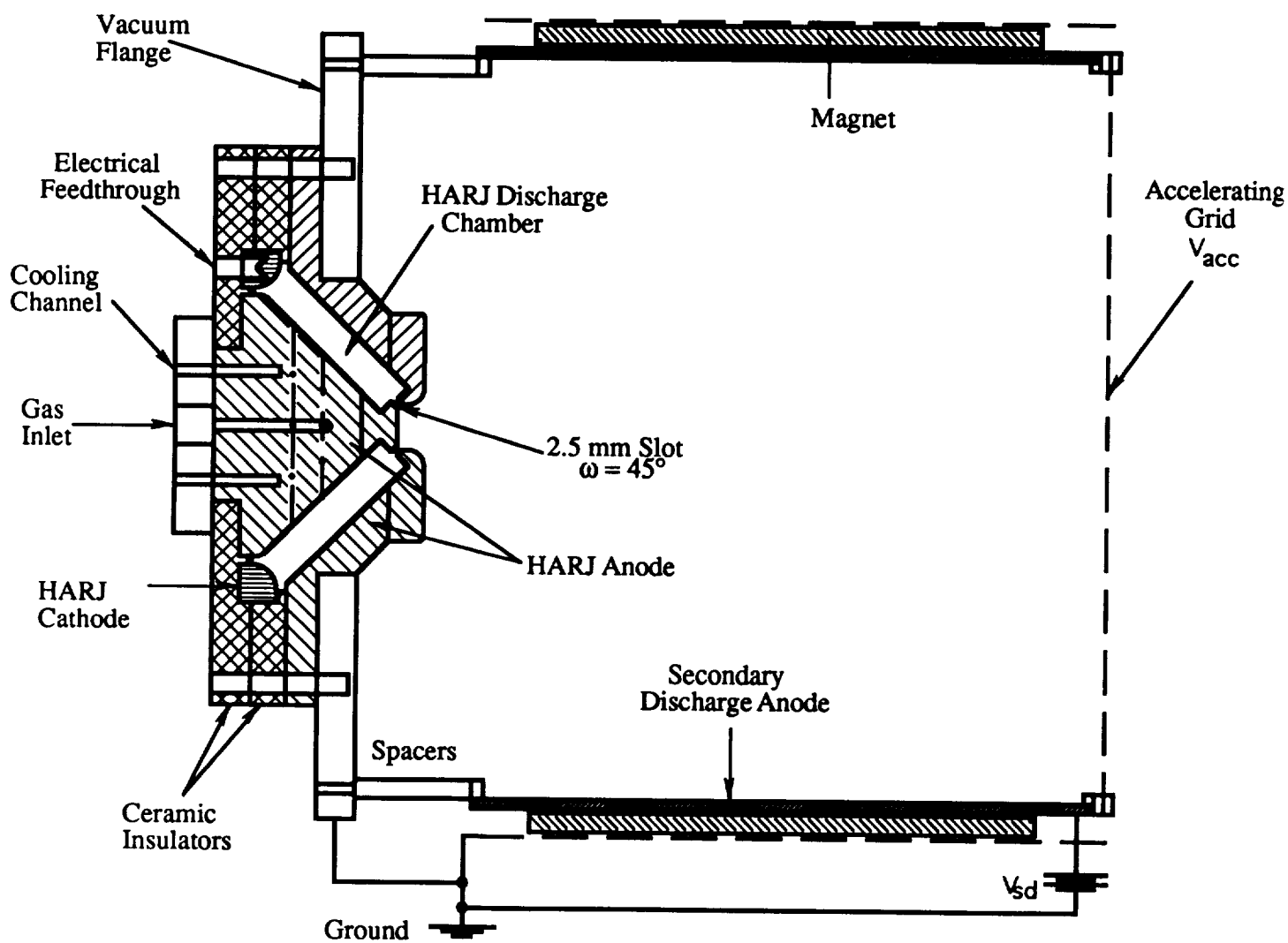


FIGURE 2
 Ion Engine (HARJ/Secondary Discharge Chamber) Schematic

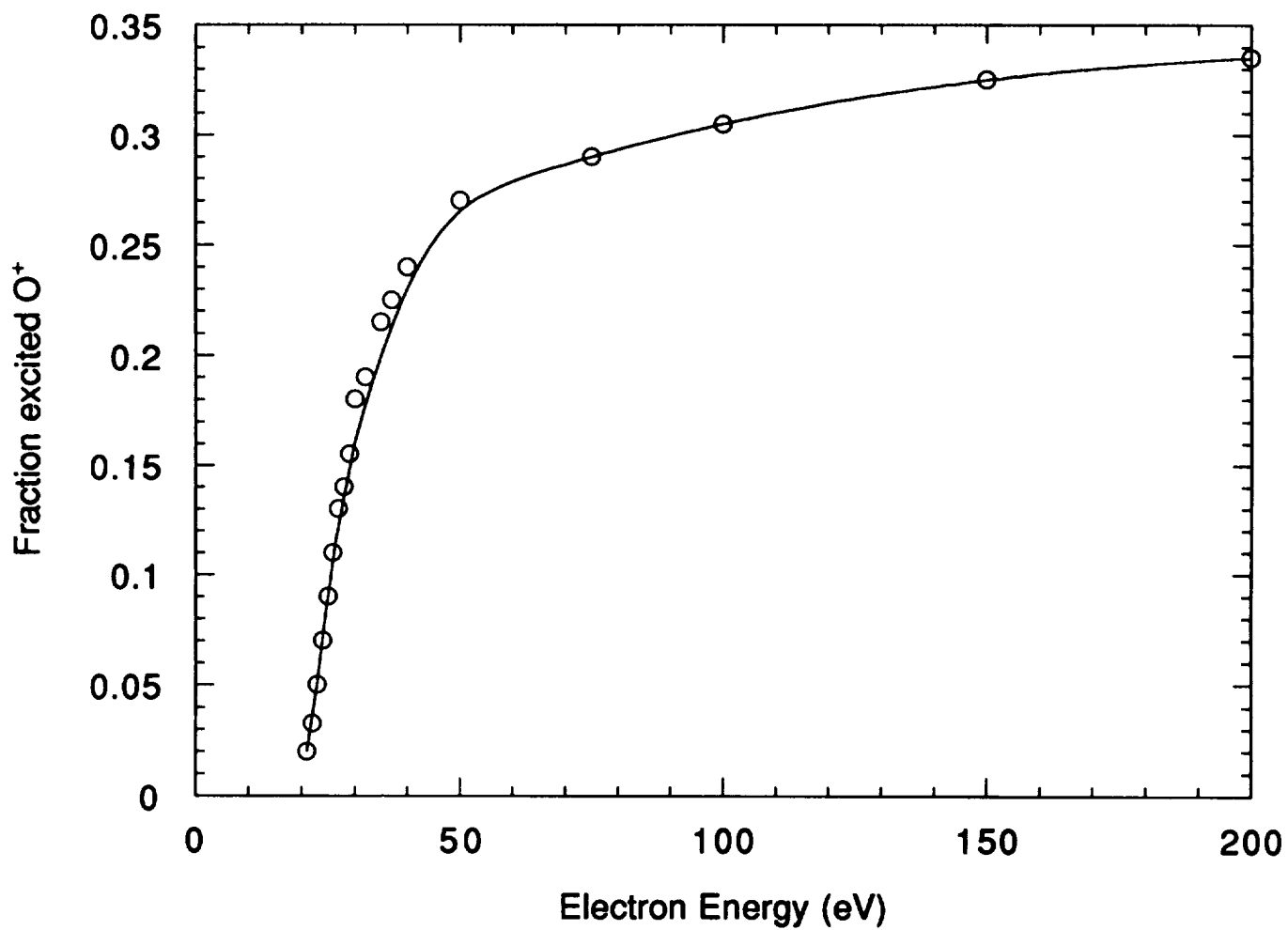


FIGURE 3

Faction of Electronically Excited State O⁺ Ions as a Function of Electron Energy in a Typical Discharge

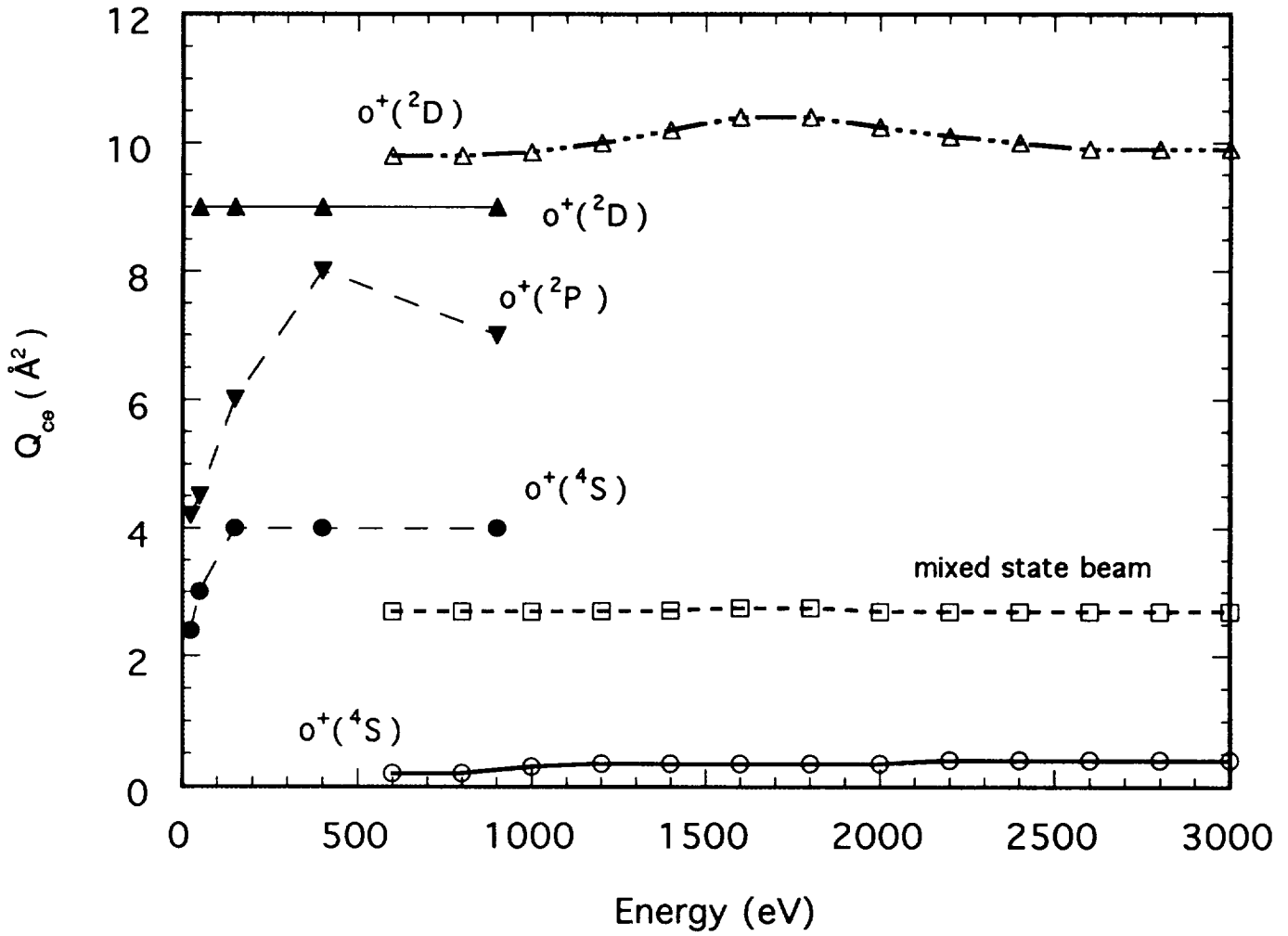


FIGURE 4

Charge Exchange Cross Sections for O^+/H_2 Reaction as a Function of Incident Ion Energy

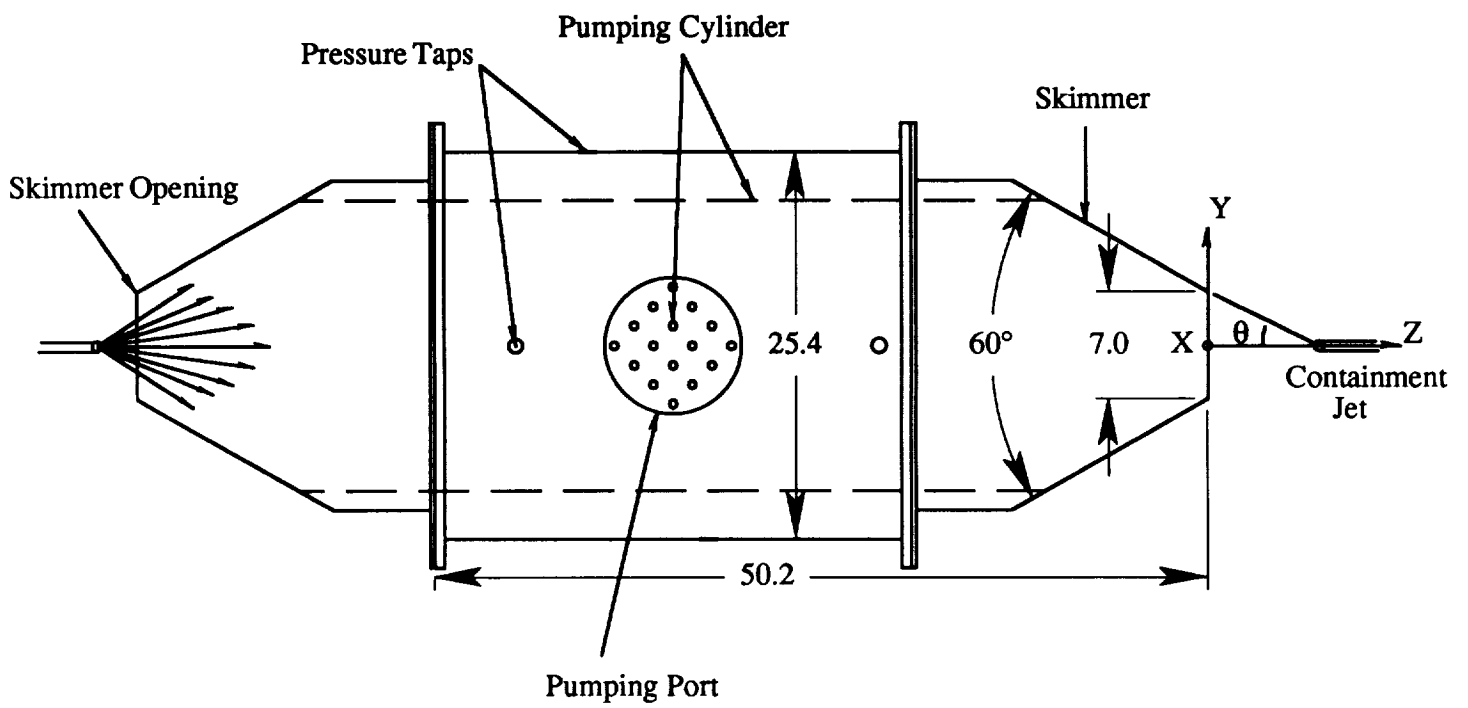


FIGURE 5
 GAITCE Schematic. All Dimensions in Centimeters.

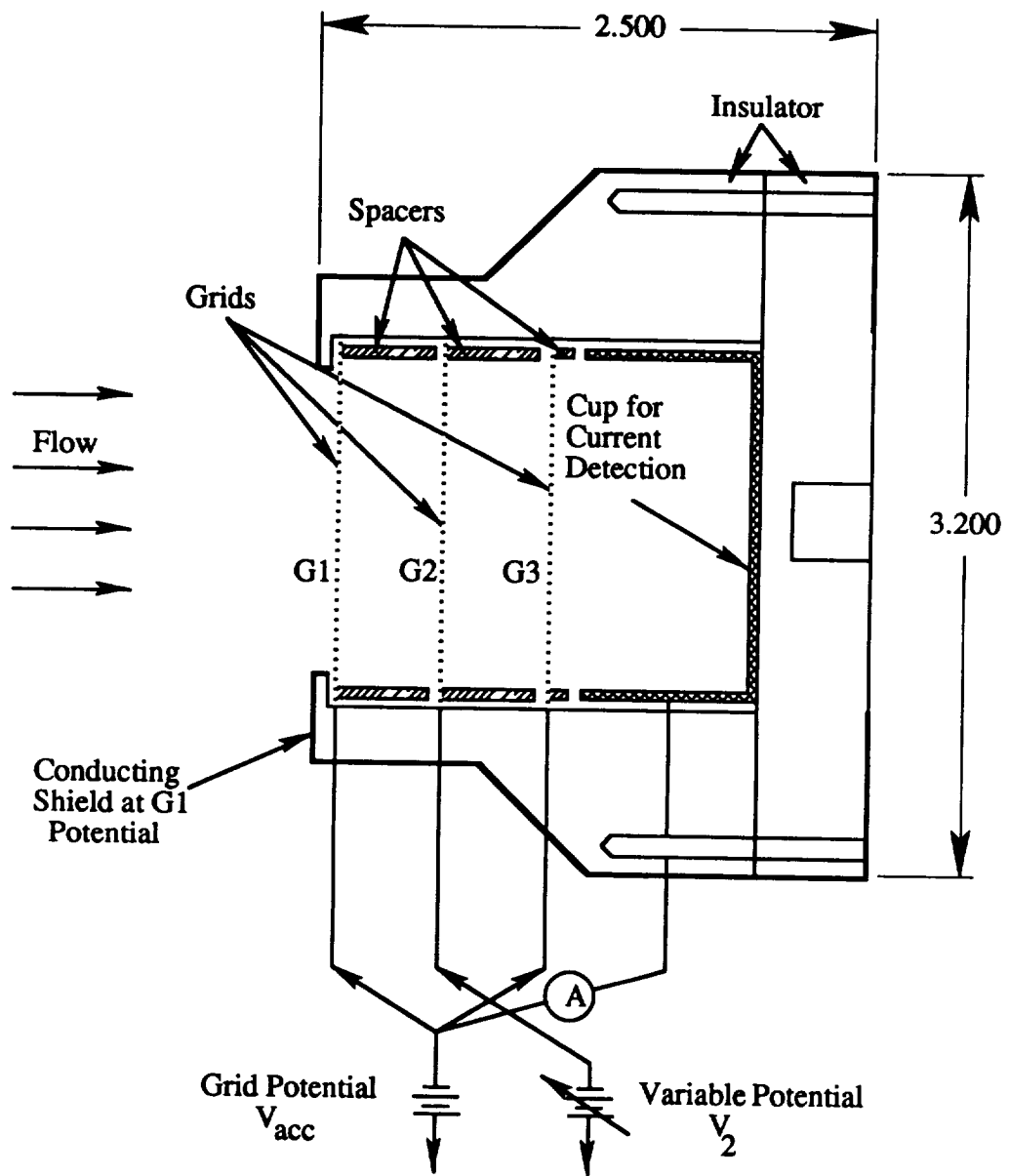


FIGURE 6
EEA Schematic. All Dimensions in Centimeters.

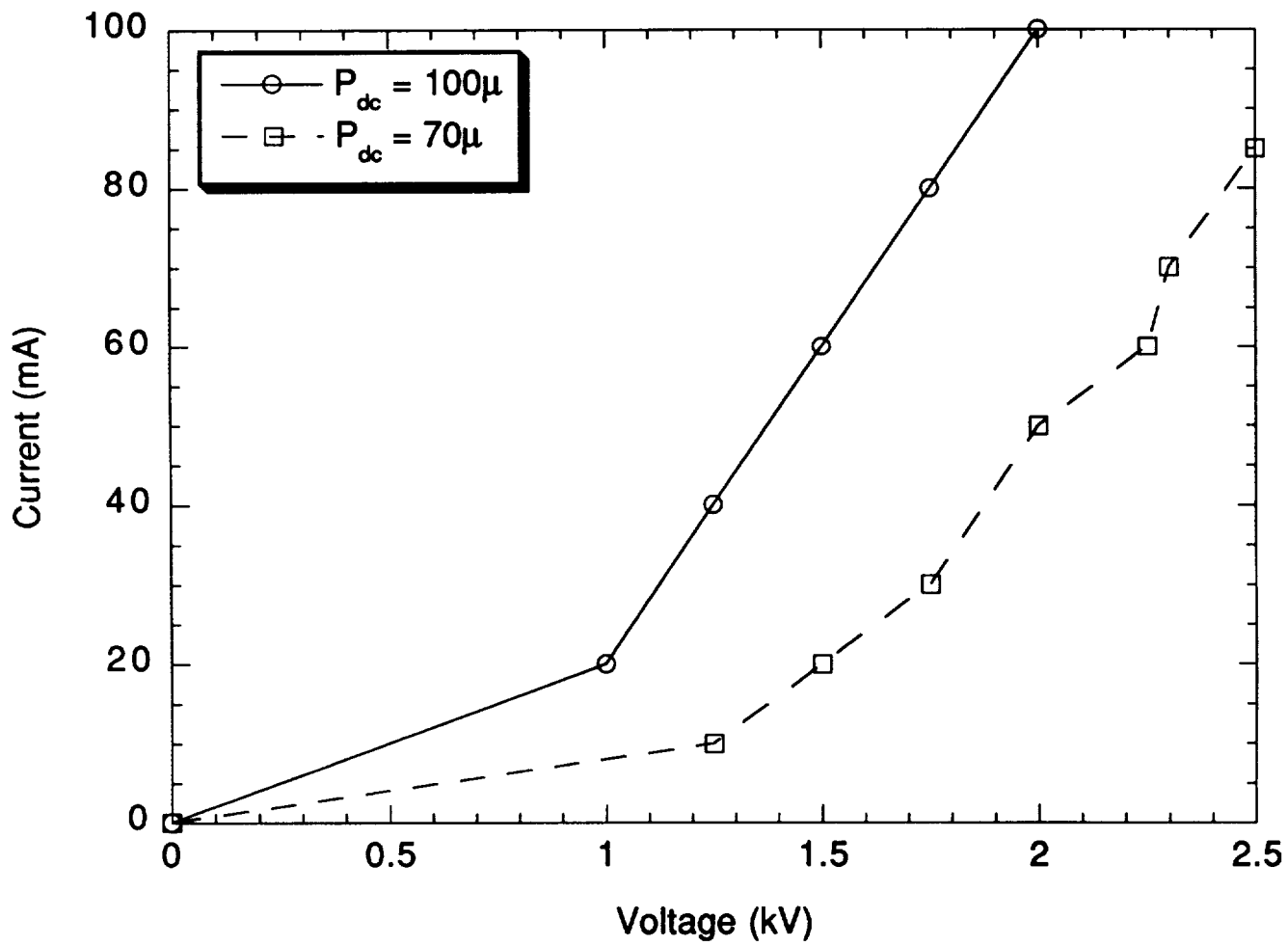


FIGURE 7
Typical HARJ Discharge Characteristics

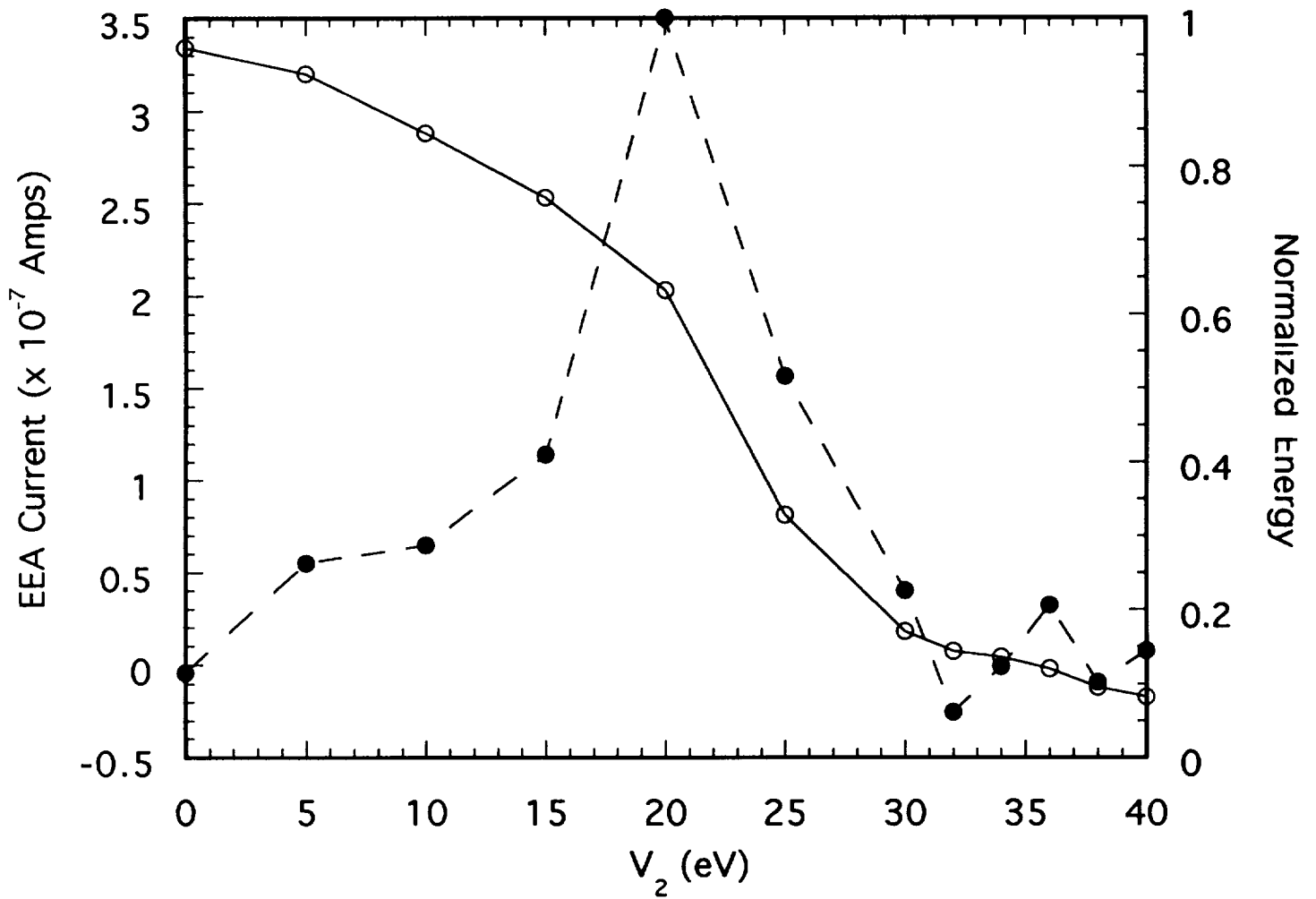


FIGURE 8

Ion Engine Current and Normalized Ion Energy versus EEA Grid 2 Voltage (V_2).
Energy: Solid Symbols.

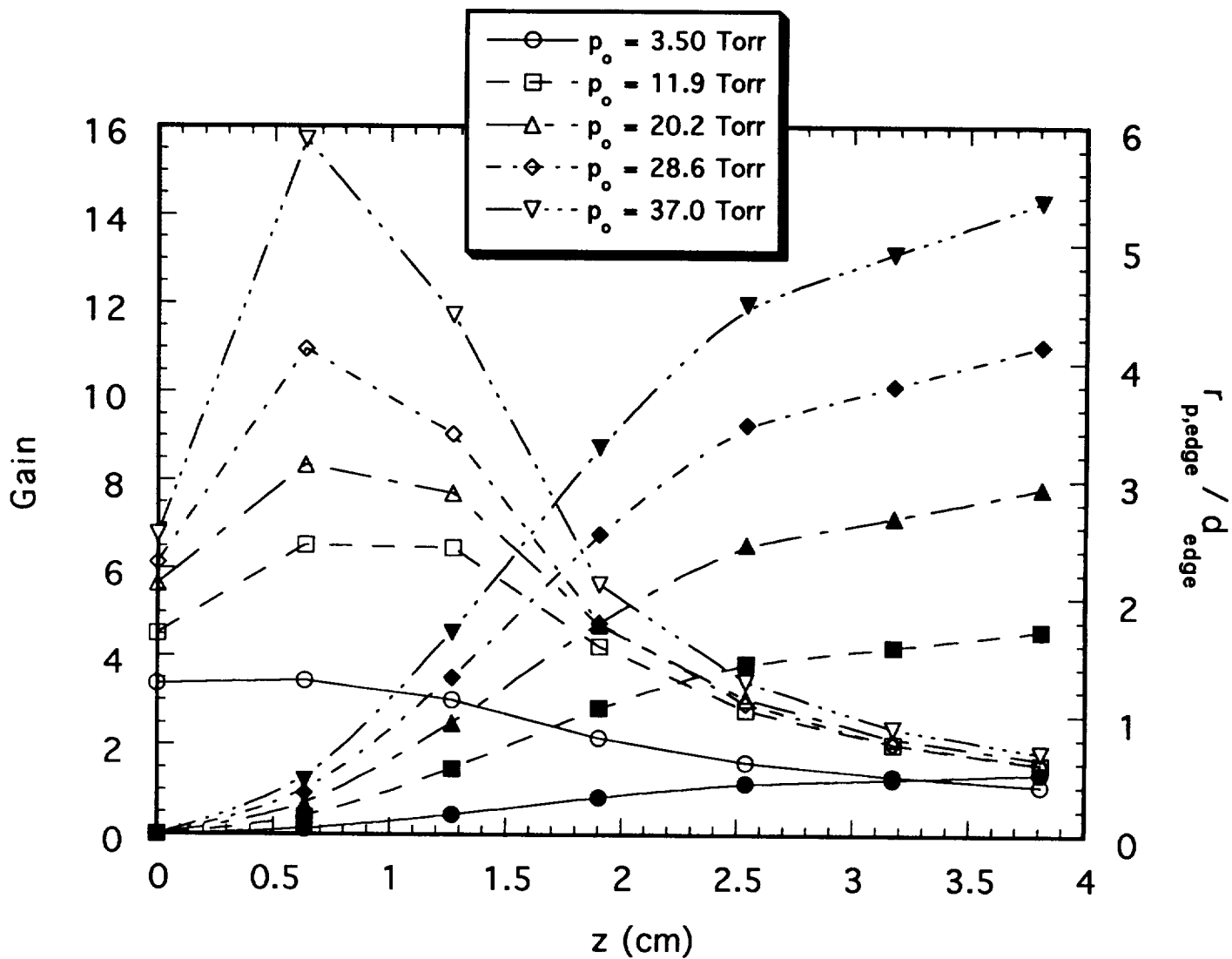


FIGURE 9

GAITCE Gain and $r_{p,edge}/d_{edge}$ as a Function of z for Various Jet Stagnation Pressures (Nitrogen). Gain: Open Symbols.